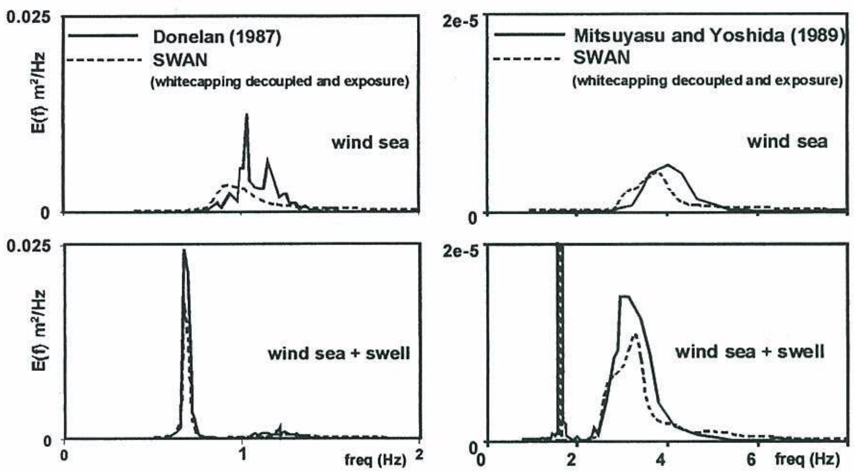

Fig. 4 The observations and the results of the SWAN model with high-frequency whitecapping decoupled from low-frequency wave steepness and with the exposure effect included.

ACKNOWLEDGEMENTS

We thank our colleague M. Yamaguchi of the Ehime University in Matsuyama (Japan) for his assistance in interpreting the paper of Mitsuyasu and Yoshida (1997, which is in Japanese). The US Office of Naval Research under Grant N00014-97-0113 supported this study. The public domain version of SWAN (swan.ct.tudelft.nl) is also supported under this grant.

REFERENCES

Donelan, M.A., 1987, The effect of swell on the growth of wind waves, *Johns Hopkins APL Technical Digest*, 8, 1, 18-23

Holthuijsen, L.H, R.C. Ris, N. Booij and E.Cecchi, 2000, Swell and whitecapping, a numerical experiment, Proc. *7th Int. Conf. Coastal Engng.*, Sydney, p. 346-354

Mitsuyasu, H. and Y. Yoshida, 1989, Air-sea interactions under the existence of swell propagating against the wind, *Bul. Res. Inst. Appl. Mech.*, Kyushu Univ. (in Japanese), 63, 47-71

Mitsuyasu, H., 1966, Interactions between water waves and wind (1), *Rep. Inst. Appl. Mech.*, Kyushu Univ., 14, 67-88

WAMDI group, 1988, The WAM model - a third generation ocean wave prediction model, *J. Phys. Oceanogr.*, **18**, 1775-1810

Wu, J., 1982: Wind-stress coefficients over sea surface from breeze to hurricane, *J. Geophys. Res.*, **87**, C12, 9704-9706

IMPROVING PROPAGATION IN OCEAN WAVE MODELS [1]

Hendrik L. Tolman [2]

Abstract Intermediate results of ongoing research at NCEP to improve the accuracy and economics of wave propagation in large-scale wind wave models are presented. The main attention is focussed of new solutions for the so-called Garden Sprinkler Effect. Also briefly discussed are the need for higher spectral resolution and plans to deal with unresolved islands by sub-grid treatment rather than by increasing spatial resolution.

INTRODUCTION

Ocean wind wave models generally solve some form of the spectral energy balance equation

$$\frac{\partial E}{\partial t} + \nabla \cdot \mathbf{c} E = S \ , \qquad (1)$$

where E represents the spectrum, $\mathbf{c}$ the advection velocities in both spectral and physical spaces, and S describes non-conservative processes. The second term on the left represents effects of propagation. In the deep ocean, effects of propagation are, from a physical perspective, simple to describe; wave energy propagates along great circles subject to dispersion in all spaces. Both propagation and dispersion are inherently linear. From a numerical perspective, however, wave propagation in the deep ocean poses major problems. In arbitrary order, the three major problems are :

[1] OMB contribution Nr. 204

[2] SAIC/GSO at NOAA/NCEP/EMC Ocean modeling Branch, 5200 Auth Road Room 209, Camp Springs, MD 21746, Hendrik.Tolman@NOAA.gov

- Selection of the numerical scheme. The scheme has to be accurate for propagation, while being positive definite (no generation of negative energy) and free of notable spurious solutions (i.e. 'wiggles'). Note that selecting a scheme with the above properties will generally also avoid most numerical problems for shallow water propagation with strong refraction (not discussed in the present paper).
- Alleviation of the so-called 'Garden Sprinkler Effect' (GSE). This subject will be discussed in detail in the following section.
- Determining and/or attaining required resolutions.

In the present paper these issues will be discussed in the context of the ocean wave model WAVEWATCH III (Tolman and Chalikov 1996, Tolman 1999), which is now the operational forecast model at NCEP. New concepts as discussed here are implemented in, and illustrated with the present experimental version of this model. New methods are also tentatively targeted for inclusion in the next public release of this model.

Although development of adequate propagation schemes is far from trivial, this problem for wave models is shared with many other fields in numerical engineering. Rather than reinventing the wheel, it makes much more sense to adopt experience from other fields from either text books like Fletcher (1988), or from comprehensive comparisons of existing schemes like Falconer and Cahyono (1993). Using such an approach, Tolman (1995) selected the third-order accurate ULTIMATE QUICKEST scheme of Leonard (1979, 1991) for use in WAVEWATCH III. Although there is always room for incremental improvement in accuracy and/or economy, this scheme at present seems satisfactory. Therefore, there appears to be no urgent need to systematically investigate numerical schemes. The present paper will therefore focus on the GSE and resolution problems in the following two sections.

GARDEN SPRINKLER EFFECT

When some form of Eq. (1) is solved in a computer model, physical and spectral space are discretized. From a historical perspective describing the spectral space with the spectral frequency f and direction θ, models like WAVEWATCH III generally use a logarithmic discretization of f,

$$f_{i+1} = \gamma f_i \tag{2}$$

where i is the discrete grid counter. Directions are generally discretized uniformly. Typical resolutions in operational models are $\gamma = 1.10$ and $\Delta\theta = 15^o$. When performing spatial propagation, discrete spectral components (f_i, θ_j) are propagated with the group velocity vector $\mathbf{c}_g$ corresponding to the average frequency and direction of the spectral bin (f_i, θ_j). Thus instead of generating continuous dispersion of swell fields, discrete swell fields are propagated in discrete directions

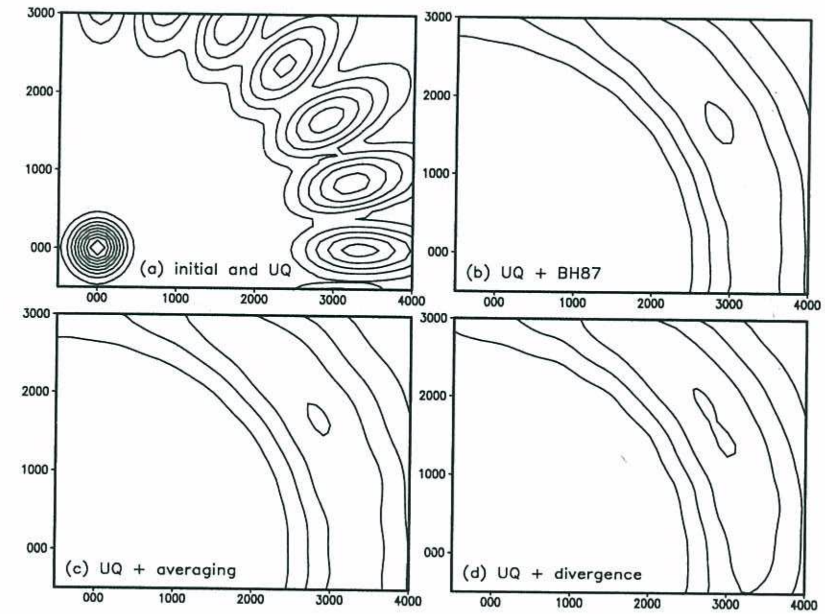

Fig. 1: GSE test adopted from Booij and Holthuijsen (1987) (BH87). See text for details. Axes in km. Contour levels at 0.25 m for inital conditions and 0.10 m otherwise.

and with discrete speeds at intervals $\Delta\theta$ and $(\gamma - 1)f$, respectively. The corresponding spurious disintegration of continuous swell fields is known as the Garden Sprinkler Effect (GSE).

The GSE is illustrated in Fig. 1 using a test case loosely based on the test case of Booij and Holthuijsen (1987, henceforth denoted as BH87). In an area of 4500×3500 km, discretized with increments of 100 km, an initial swell field is placed 500 km from the lower and left sides. The initial maximum wave height $H_s = 2.5$ m. The wave height distribution is Gaussian in physical space with a spread of 150 km. The mean spectral direction is 30° (Cartesian) with a directional distribution of the type $\cos^2$. The peak frequency is 0.1 Hz, and the frequency spectrum is of Gaussian shape with a spread of 0.005 Hz. The spectral discretization is defined by $\gamma = 1.10$ and $\Delta\theta = 15^o$. Fig. 1 shows initial conditions (panel a), and results after 5 days of propagation for several numerical approaches. Fig. 1a shows the results of the ULTIMATE QUICKEST (UQ) scheme, clearly displaying the GSE. The exact solution without the GSE is not shown here, but is close to Fig. 1d.

Booij and Holthuijsen (1987) suggested a solution to the GSE, adding a diffusion tensor to the propagation equation (1). For a Cartesian (x,y) grid as used in the test, the modified equation is

$$\frac{\partial E}{\partial t} + \frac{\partial}{\partial x}\left[c_x E - D_{xx}\frac{\partial E}{\partial x}\right] + \frac{\partial}{\partial y}\left[c_y E - D_{yy}\frac{\partial E}{\partial y}\right] - 2D_{xy}\frac{\partial^2 E}{\partial x \partial y} = S \ , \qquad (3)$$

where D_{xx}, D_{yy} and D_{xy} represent a diffusion tensor, the main axis of which lines up with θ (see BH87 for details). Compared to Eq. (1), Eq. (3) adds a directional diffusion to the propagation equation. Formally the strength of this diffusion increases linearly with the time passed since the generation of the wave energy (T_s, see BH87 for details). At the suggestion of BH87, T_s is kept constant in WAVEWATCH III, to avoid significant increases in computational costs and memory requirements. Effectively, T_s then becomes a tunable parameter. Figure 3b shows results for the UQ scheme with the added diffusion terms and T_s = 5 days. Indeed, the GSE has been removed, and the solution closely resembles the exact solution (close to Fig. 1d).

The BH87 solution to the GSE has been shown to be necessary and practical in the operational implementations of WAVEWATCH III at NCEP. There is, however, one major drawback. In the advection part of Eq. (3), the maximum allowed numerical time step $\Delta t_{\max}$ scales with the grid step as Δx^{-1}. For the diffusion part, however, $\Delta t_{\max}$ scales with Δx^{-2}. Thus, the diffusion component of the equation will dictate acceptable time steps for sufficiently high resolution. For NCEP's global wave model, with a spatial resolution of approximately[3] 100 km, the required time step for advection allows for the required T_s = 4 days. Adding the GSE correction then results in a acceptable increase of computational time of about 15%. For the regional models with a resolution of approximately 25 km, the required advection time step allows for $T_s \approx$ 24 h. This setting is borderline acceptable for models driven with large-scale wind field. For the regional North Atlantic Hurricane model (NAH), however, the high-resolution forcing requires $T_s \approx$ 72 h for properly smoothed results. The necessary reduction of propagation time step results in a model that takes about 75% more computational time than a model without the BH87 GSE correction. This increased model run time has lead us to search for alternatives to the BH87 GSE solution.

The GSE occurs because the energy contained within a spectral bin is propagated with its mean velocity without the proper dispersion in space. Any solution to this problem has to explicitly deal with sub-grid dispersion. Averaging over the actual bin space generally does not help, as the averaged equations generally reproduce the discrete propagation with the mean parameters of the spectral bin only. Two alternatives have been considered here. The first mimics sub-grid dispersion by spatial averaging over a controlled area. The second mimics dispersion by adding divergence to the advection velocities.

[3] Actual grid 1.25° × 1.00° in longitude and latitude.

Considering that the spectral bin (f_i, θ_j) in fact contains wave energy in a band $(\Delta f, \Delta\theta)$ around (f_i, θ_j), the advection velocities will vary similarly. Thus, energy at some spatial location is not simply advected by $\mathbf{c}_g\Delta t$, but is spread in the propagation direction over an area $\Delta\mathbf{c}_g\Delta t$, and in the perpendicular direction over $\mathbf{c}_g\Delta\theta\Delta t$ around $\mathbf{c}_g\Delta t$ (in a simple linearized approximation). A simple way of modelling this is to average the advected wave field over such an area before or after the actual numerical propagation is performed. Note that the distinct orientation of such an averaging area closely resembles that tensor nature of the diffusion in BH87. This method can be made tunable by adding multiplication factors to the size of the averaging area in the propagation and perpendicular directions. The method is also obviously sensitive to the actual averaging algorithm.

In the present test version of WAVEWATCH III, the UQ scheme with pre-averaging has been included to test this concept. The averaging is performed by averaging the wave energy at the four corner points of a box of size $\alpha_s\Delta\mathbf{c}_g\Delta t \times \alpha_n\mathbf{c}_g\Delta\theta\Delta t$ around each grid point, where the wave energy is estimated using bi-linear interpolation from the spatial grid. The multiplication factors α_s and α_n are added to provide tuning capability. In the present calculations, these factors are set to 2.0. Results of the propagation test with these model settings are shown in Fig. 1c. Clearly, the simple averaging technique gives model results very similar to those of the BH87 diffusive correction (panel b). The averaging, however, has no impact on required time steps. Furthermore, it may be expected that the tuning of this model is fairly general, unlike for the BH87 solution, where T_s needs to represent a typical propagation time of swell through the area.

Another way of introducing dispersion of wave energy in space is to add some divergence to the advection field $\mathbf{c}_g$. Consider again, that the energy at a given bin (f_i, θ_j) in fact contains wave energy in a band $(\Delta f, \Delta\theta)$. Energy at lower frequencies than f_i will travel faster, and will end up at the front of the swell field described by (f_i, θ_j). Energy at higher frequencies similarly will end up at the back of the swell field, and energy in the bin to the left or right of θ_j will end up on the corresponding side of the swell field. This process can simply be modeled by adding a systematic divergence to the advection field. In the test version of WAVEWATCH III, the following algorithm has been included.

a) Find the maximum energy $E_{\max}$ and its location for the bin considered.

b) Determine the spatial extent of the corresponding swell field in the propagation ($\tilde{r}_s$) and normal ($\tilde{r}_n$) directions. Due to the general occurrence of noise in models, this extend is determined by checking where $E(f_i, \theta_j; x, y) < \beta_0 E_{\max})$, with $\beta_0 > 0$.

c) Correct the original propagation velocity $c_{g,0}$ and direction θ_0 as follows

$$c_g = c_{g,0} + 0.5\beta_s\frac{r_s}{\tilde{r}_s}\Delta c_g \ , \qquad (4)$$

$$\theta = \theta_0 + 0.5\beta_n \frac{r_n}{\tilde{r}_n} \Delta\theta \ , \qquad (5)$$

where r_s and r_n are the distances of the grid point to the location of maximum energy in propagation and normal direction, respectively.

β_0, β_s and β_n again allow for some tuning. Note that for the test case of Fig. 1 this algorithm is easily implemented, because for each bin (f_i, θ_j) only one swell field is available. In practical conditions, however, multiple swell fields are expected, and the above algorithm has to be applied iteratively to individual swell fields. Figure 1d shows results for this algorithm with $\beta_0 = 0.05$, and $\beta_n = \beta_s = 1.2$. This algorithm shows more properly smoothed results than the BH87 and averaging methods (panels b and c, respectively). This can be explained by the fact that the divergent algorithm adds proper curvature to the swell fields of individual bins, whereas the other two algorithms redistribute energy along main axes only, without adding curvature.

The test case of Fig. 1 clearly demonstrates the GSE and its solutions, but it does not address the necessity or economical impact of the GSE solutions in practical conditions. The GSE is most likely to occur in models with high-resolution forcing in space and time. At NCEP, the model therefore most sensitive is the North Atlantic Hurricane (NAH) wave model. To illustrate the practical impact of the GSE and its solutions, results for the NAH model for hurricane Florence are presented in Fig. 2. Due to the coexistence of multiple wave fields, the GSE is not necessarily obvious in wave height fields. It is, however, obvious in the peak period (T_p) fields. The peak period is defined as the period corresponding to the highest peak in the one-dimensional spectrum $E(f)$. Peak periods are presented in Fig. 2 for the UQ scheme without GSE correction (panel a), the UQ scheme with the BH87 correction with $T_s = 3$ days (panel b, standard NAH model), and for the averaging (panel c) and divergent advection (panel d) solutions with settings identical to those used in Fig. 1.

For the UQ scheme without GSE mitigation (Fig. 2a), the occurrence of the GSE is obvious in the 'spokes of a wheel' type structure of the T_p fields. For clarity of display, contours are not labeled in this panel. The 'spokes' are much more elongated than in Fig. 1 due to the much broader range of energy carrying frequencies, and due to the nature of the parameter displayed (T_p versus H_s, T_p generally has a distinct signature even far away from the area with maximum H_s). All three methods to suppress the GSE (panels b through d) show very similar results. Because no exact solution is available, it is impossible to identify one as 'most correct'. Some of the differences between the models could be removed by modifying the available tuning parameters. With the present setting of tuning parameters, the GSE correction of BH87 (operational NAH model) gives the smoothest fields of T_p. Some evidence of extraneous smoothing can be found in the fact that the resolved islands in the Bahamas (around 25°N and 76°W) show no evidence of shadowing, whereas such shadowing can be observed with the

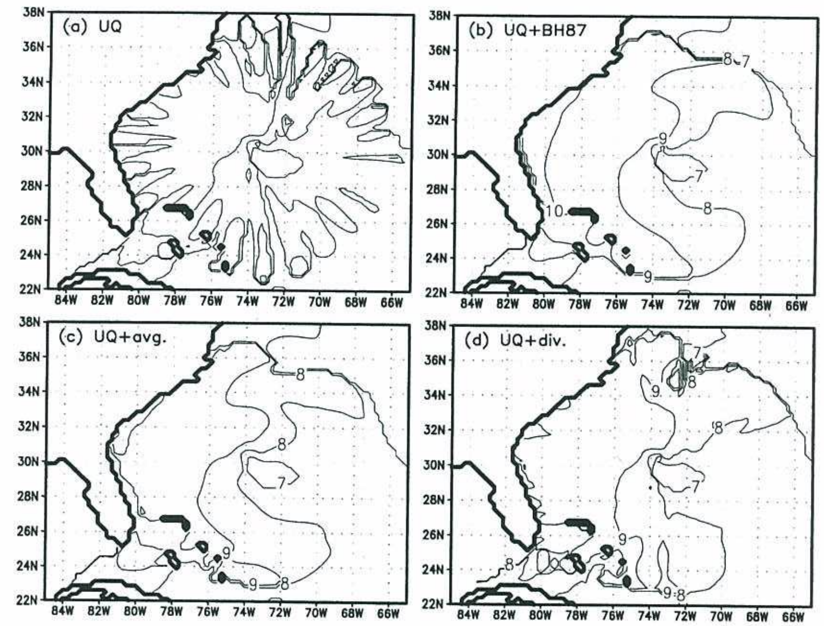

Fig. 2: Peak periods T_p in seconds for hurricane Florence from NAH model, Sept. 13 2000, 0 UTC. Numerical methods as indicated in panels. Thick line is land-sea boundary of model.

averaging and divergent field methods (panels c and d).

With the very similar results for all three GSE corrections, their economics become important. Compared to the plain UQ scheme, the BH87 solution resulted in a 75% increase in computational time. As discussed above, this is mostly due to the need to run with smaller discrete time steps. If T_s is chosen sufficiently small not to influence the time step, an increase of computational time of 15% is found. The averaging technique results in a moderate increase of computational time of 11%. Due to its nature, it does not impact the required time steps. A timing of the divergent advection field method is difficult to obtain. The costs of this method depend mostly on the efficiency of the decomposition of the combined wave field for $E(f_i, \theta_j)$ in individual swell fields in space. This has not yet been investigated in detail. The present results were obtained at a 75% increase in computational time compared to the plain UQ scheme. Although the efficiency might be improved, the inherently complex nature of the decomposition is always expected to be significantly more expensive than the simple averaging method. Moreover, this method reduces the required time step by a factor of roughly γ^{-1} due to systematically increase advections velocities.

MODEL RESOLUTION

The past decade has seen a systematic increase of spatial resolution of operational wave models at virtually every major operational forecast center. Simultaneously, spectral resolutions have largely remained unchanged at $\gamma = 1.10$ and $\Delta\theta = 15^o$. This potential imbalance in increasing resolutions has not been discussed in much detail.

Lack of spectral resolution, in particular in directions, leads to the GSE as discussed in detail in the previous section and in BH87. Fortunately, 'sub-grid' methods can alleviate the GSE, and thus avoid the need to increase directional resolution in order to get physically realistic results. The present spectral resolutions in frequency and direction furthermore appear adequate to describe wave growth (e.g., Tolman 1992). The frequency resolution, however, is generally inadequate to describe details of the spectral peak. As is illustrated in Figs. 26 and 27 of Tolman (1995), this leads to a systematic inability of the wave models to describe swell dispersion adequately. This inability is not alleviated by GSE solutions, and therefore appears to require a systematic increase of frequency resolution in the models. This might have a notable impact on the arrival time and height of swell fronts. Swell prediction has increasingly been recognized as a critical aspect of operational wave forecasting. Swell heights, however, are generally not dominating overall wave heights. Therefore, improvement of swell forecasts generally has a negligible impact on conventional wave height validation statistics. Additional validation parameters concentrating on swell should be considered to supplement conventional validation parameters.

Spatial resolution is required for two reasons. First, the resolution needs to be equal to, or better than the resolution of the driving wind fields. This appears to have driven the increase in spatial resolutions of wave models in the recent past. The second reason is the need to describe coastlines adequately. This is illustrated here in Fig. 3, which shows the scatter index (rms error normalized with mean observation) of part of NCEP's global NWW3 model for a three-month period in 1998. In the open ocean, the scatter index is typically 15%. Figure 3, however, shows much larger scatter indices of up to 30% near French Polynesia (15°S - 135°W) and around the Solomon and adjacent island groups (10°S - 160°E). Because these island groups are not resolved in the model, swell in the model travels past them. In nature this swell energy is dissipated at the shores. Similar model behavior can be observed at many other unresolved island groups (figures not presented here). This model deficiency can easily be removed by increasing spatial resolution.

However, particularly in French Polynesia, Fig. 3 illustrates the need for unrealistically high resolutions to resolve this problem adequately. Proper resolution of many atolls would require a spatial resolution of well below 10 km. Moreover, this resolution would be required only near the islands. Away from the islands,

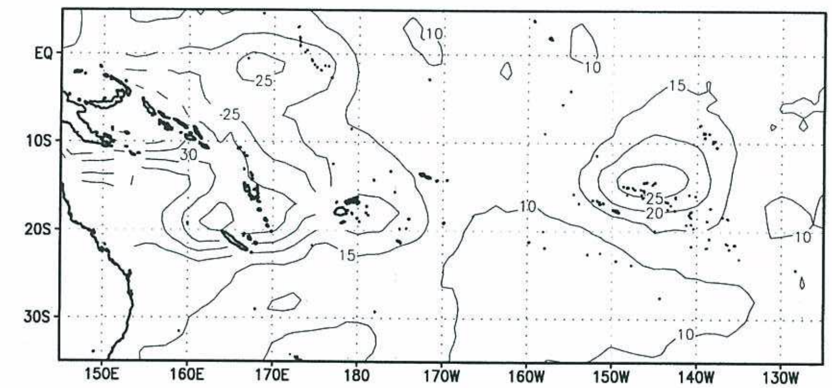

Fig. 3: Wave height scatter index in % of part of the global NWW3 model against ERS-2 altimeter for March through May 1998. Thick lines depict continents and islands from external sources (i.e., not necessarily seen by model).

the wind field resolution still dictates the required wave model resolution. Alternatively, unresolved islands can be treated at a subgrid level as a partial barrier. Such a methodology has already been included in the SWAN model (Booij et al 1999) for explicitly defined barriers. Considering that in WAVEWATCH III all numerical propagation schemes are expressed in terms of fluxes through cell boundaries, cell boundary transparencies can easily be included as a corresponding suppression of numerical energy fluxes going into a cell only. Such a methodology has been included in the experimental version of WAVEWATCH III, and will be tested in NCEP's global and regional wave models in the near future.

SUMMARY AND CONCLUSIONS

Three major problems with wave propagation in ocean wave modeling have been identified; the basic numerical scheme used, the Garden Sprinkler Effect (GSE) and the lack of proper numerical resolution. For the development and selection of numerical schemes, experience from other fields can, and has been used. The other two issues are discussed here in some detail.

The GSE results in aphysical model behavior for practical models as is illustrated here in Fig. 2a with results of NCEP's NAH model for hurricane Florence. WAVEWATCH III as presently used in the NAH model uses the diffusive correction method of Booij and Holthuijsen (1987, BH87) to mitigate the GSE successfully (Fig. 2b), at a cost of a 75% increase in computational time. Two alternatives are presented here. An averaging technique (Fig. 2b) also mitigates the GSE, but at a cost increase of only 11% in model run time. A divergent advection field method gives better results in an idealized test due to the more physically correct shape of the correction (Fig. 1d), but proves expensive for practical applications (65% increase in costs for present approach).

Two reasons exist for increasing model resolution. Better frequency resolution is required to properly describe the spectral peak and swell dispersion. Spatial resolution needs to keep up with increasing spatial resolution of atmospheric models that provide driving forces for the wave models. For both reasons to increase resolution, no subgrid alternatives are available. Present models also require higher spatial resolution for resolving island groups properly. This problem, however, should first be approached from a sub-grid perspective, rather than by (locally) increasing the spatial model resolution.

ACKNOWLEDGEMENTS

The author would like to thank Larry Burroughs for constructive comments on early drafts of this manuscript. The present study was made possibly by funding from the NOAA High Performance Computing and Communication (HPCC) office.

REFERENCES

Booij, N. and L.H. Holthuijsen, 1987. Propagation of ocean waves in discrete spectral wave models. *J. Comput. Phys.*, **68**, 307-326.

Booij, N., R.C. Ris and L.H. Holthuijsen, 1999. A third-generation wave model for coastal regions, Part I, Model description and validation, *J. Geophys. Res.*, **104**, 7649-7666.

Falconer, R.A., and Cahyono, 1993. Water quality modelling in well mixed estuaries using higher order accurate differencing schemes. Advances in hydroscience and engineering, S.S.Y. Wang Ed., 81-92.

Fletcher, C.A.J., 1988. *Computational techniques for fluid dynamics, part I and II.* Springer, 409+484 pp.

Leonard, B.P., 1979. A stable and accurate convective modelling procedure based on quadratic upstream interpolation. *Comput. Methods Appl. Mech. Engng*, **18**, 59-98.

Leonard, B.P., 1991. The ULTIMATE conservative difference scheme applied to unsteady one-dimensional advection. *Comput. Methods Appl. Mech. Engng.*, **88**, 17-74.

Tolman, H.L., 1992. Effects of numerics on the physics in a third-generation wind-wave model. *J. Phys. Oceanogr.*, **22**, 1095-1111.

Tolman, H.L., 1995. On the selection of propagation schemes for a spectral wind-wave model. NWS/NCEP Office Note 411, 30pp. + figures.

Tolman, H.L., 1999. User manual and system documentation of WAVEWATCH III version 1.18. NOAA/NWS/NCEP/OMB Techn. Note 166, Available from http://polar.ncep.noaa.gov/waves/wavewatch.

Tolman, H.L., and D.V. Chalikov, 1996. Source terms in a third-generation wind wave model. *J. Phys. Oceanogr.*, 26 (1996) 2497-2518.

DIRECTIONAL SPREADING IN OCEAN SWELL

Kevin C. Ewans[1]

Abstract: Directional wave spectra derived from a data set measured off the west coast of New Zealand are used to investigate the directional spreading within swell. The location where the measurements were made is particularly useful for the study as a more or less constant swell component originating from the Southern Ocean is observed in the sea states. The spectra are partitioned into wind-sea and swell components, and estimates of the directional spreading of the swell component is made. A function for the directional distribution of the swell is proposed.

INTRODUCTION

The wave directional distribution is an important quantity in wave forecasting and in the design and operation of offshore engineering facilities. Considerable effort has focused on the directional distribution of active wind-seas, resulting in significant improvement in the understanding of directionality during wave growth. In most regions around the world, the extreme sea states for which offshore facilities must be engineered are also associated with active wind-seas.

However, there are locations, such as offshore West Africa, and offshore operations for which swell is equally if not more important. For example, swell governs the wave design criteria offshore Nigeria, and the persistent swell from the Southern Ocean has an important influence on the workability of vessels off the west coast of New Zealand. But the directionality of swell, and particularly the spreading in swell, has received far less attention than the wind-sea component.

The paper reports an evaluation of a wave directional data set, recorded off the west coast of New Zealand. The spectra are partitioned into wind-sea and swell components, characteristics of the swell spreading are established, and a swell spreading function is developed.

1 K. C. Ewans Metocean Engineer, Offshore Technology, Upstream Sector, Shell Global Solutions International B.V., P.O. Box 60, 2280 AB Rijswijk, The Netherlands, k.ewans@siep.shell.com